Inorganic Chemistry

ARTICLE

pubs.acs.org/IC

Synthesis, Structural Charaterization, and Electrochemical and Optical Properties of Ferrocene−Triazole−Pyridine Triads

Tomás Romero,[†] Raúl A. Orenes,[‡] Arturo Espinosa,[†] Alberto Tárraga,[*,†] and Pedro Molina[*,†]

[†]Departamento de Química Orgánica, Facultad de Química, and [‡]Servicio de Apoyo a la Investigación (SAI), Campus de Espinardo, Universidad de Murcia, E-30100 Murcia, Spain

S *Supporting Information*

ABSTRACT: The synthesis and electrochemical, optical, and cation-sensing properties of the ferrocene−triazole−pyridine triads **3** and **5** are presented. Azidoferrocene **1** and 1,1′-diazidoferrocene **4** underwent the "click" reaction with 2-ethynylpyridine to give the triads **3** and **5** in 81% and 68% yield, respectively. Electrochemical studies carried out in CH_3CN in the presence of increasing amounts of Zn^{2+}, Ni^{2+}, Cd^{2+}, Hg^{2+}, and Pb^{2+} metal cations, showed that the wave corresponding to the ferrocene/ferrocenium redox couple is anodically shifted by 70−130 mV for triad **3** and 167−214 mV for triad **5**. The maximum shift of the ferrocene oxidation wave was found for **5** in the presence of Zn^{2+}. In addition, the low-energy band of the absorption spectra of **3** and **5** are red-shifted ($\Delta\lambda$ = 5−10 nm) upon complexation with these metal cations. The crystal structures of compounds **3** and **5** and the complex $[\mathbf{3}_2\cdot\text{Zn}]^{2+}$ have been determined by single-crystal X-ray methods. ^{1}H NMR studies as well as density functional theory calculations have been carried out to get information about the binding sites that are involved in the complexation process.

INTRODUCTION

The independent discoveries of the copper(I)-catalyzed Huisgen 1,3-dipolar cycloaddition (CuAAC)[1] by Sharpless and Medal[2] have led to thousands of new examples of this reaction subclass. The excellent regioselectivity for the 1,4 isomer of the 1,2,3-triazole and the enhanced reactivity of the copper(I)-catalyzed process, along with the versatility of the reaction conditions, have made it the flagship reaction of the Sharpless "click" chemistry.[3] Furthermore, the development of the CuAAC reaction has led to renewed interest in the coordination chemistry of 1,4-functionalized 1,2,3-triazoles because they have the potential to act as nitrogen-donor ligands. In this context and in addition to its role as a structural linkage between two components, the 1,2,3-triazol-1,4-diyl moiety has also recently been highlighted as a ligand for metal ions[4] in sensing,[5] luminescence,[6] and magnetism.[7]

Recently, several communications making use of flexible triazolophanes,[8] a triazole-based cyclic peptide,[9] and a preorganized and rigid triazole-based macrocycle,[10] showing self-assembly as well as the anion binding properties of foldamers[11] and a ferrocene−triazole−pyridine system,[12] all demonstrate 1,2,3-triazoles participating in noncovalent interactions. Interestingly, 1,2,3-triazole-linked dendrimers also showed the ability of binding oxo anions through the 1,2,3-triazole ring localized inside the dendrimers.[13]

Historically, polypyridine ligands such as 2,2′-bipyridines have been essential in the development of self-assembled architectures[14] such as helicates,[15] cages,[16] and grids.[17] However, their synthesis and functionalization may be somewhat cumbersome, involving toxic reagents and extensive purification. As a result, replacing a pyridine with a triazole becomes attractive because of the easy access to starting materials and the facile functionalization via the N1 nitrogen. Surprisingly, a systematic study of coordination of the triazole−pyridine diad has not yet been reported, particularly in solution, where self-assembly expresses its full potential, and only isolated examples have been reported.[6c,18]

On the basis of such precedents, here we report the synthesis of two new chemical probes, **3** and **5**, in which a ferrocene moiety is functionalized at the 1 or 1,1′positions by one or two 4-pyridyl-1,2,3-triazol-1-yl units, respectively. In these structures, the presence of two nitrogen-coordinating atoms, with optimal orientation in order to constitute a cavity suited for hosting cationic species, and a redox-active ferrocene unit are combined. As a consequence, they allow an investigation of their coordination abilities toward several metal cations by using electrochemical and spectroscopic techniques.

EXPERIMENTAL SECTION

General Comments. Melting points were determined on a hot-plate melting point apparatus and are uncorrected. ^{1}H NMR spectra were recorded at 400 and 300 MHz, and ^{13}C NMR spectra were recorded at 150 and 100 MHz. Chemical shifts refer to signals of tetramethylsilane. The following abbreviations are used to represent the multiplicity of the signals: s (singlet), d (doublet), dd (double doublet), dt (double triplet), ddd (double doublet of doublets), st (pseudotriplet), td (triple doublet), q (quaternary carbon atom).

UV−vis spectra were carried out in a UV−vis−near-IR spectrophotometer using a dissolution cell of 10 mm path length. The samples were solved in CH_3CN ($[\mathbf{3}] = 1 \times 10^{-4}$ M and $[\mathbf{5}] = 5 \times 10^{-5}$ M), and

Received: April 11, 2011
Published: August 10, 2011

the spectra were recorded with the spectral background corrected before and after of the sequential additions of aliquots of cations in CH_3CN ($c = 2.5 \times 10^{-2}$ M).

Cyclic voltammetry (CV) and Osteryoung square-wave voltammetry (OSWV) techniques were performed with a conventional three-electrode configuration consisting of platinum working and auxiliary electrodes and a Ag/AgCl reference electrode. The experiments were carried out with a 10^{-4} M solution of the sample in CH_3CN containing 0.1 M $[(n\text{-}C_4H_9)_4N]PF_6$ ($TBAPF_6$) as the supporting electrolyte. All of the potential values reported are relative to the decamethylferrocene (DMFc) couple at room temperature.[19] Deoxygenation of the solutions was achieved by bubbling nitrogen for at least 10 min, and the working electrode was cleaned after each run. The cyclic voltammograms were recorded with a scan rate increasing from 0.05 to 1.00 V/s, while the OSWV plots were recorded at a scan rate of 100 mV/s with a pulse hight of 10 mV and a step time of 50 ms. Typically, the receptor (1×10^{-4} M) was dissolved in CH_3CN (5 mL), and $TBAPF_6$ (base electrolyte; 0.194 g) was added. The guest under investigation was then added as a 2.5×10^{-2} M solution in CH_3CN using a microsyringe, while the CV properties of the solution were monitored. DMFc was used as an external reference both for potential calibration and for reversibility criteria.

Ferrocenylazide (1). Ferrocene (2.00 g, 10.75 mmol) and potassium *tert*-butoxide (0.147 g, 1.31 mmol) were dissolved in dry tetrahydrofuran (THF; 85 mL) and cooled to −78 °C under nitrogen. Then, ^{t}BuLi (1.7 M, in pentane; 12.7 mL, 21.6 mmol) was added dropwise over 40 min. The reaction mixture was kept at −78 °C for 1.5 h and later at room temperature for 1 h. Subsequently, this solution was cooled to −55 °C and transferred dropwise via cannula under nitrogen, to a previously cooled (−55 °C) THF solution (55 mL) of 2,4,6-triisopropylbenzenesulfonylazide (3.33 g, 10.76 mmol), over 50 min. After stirring at −55 °C for 1 h, water was added and the resulting mixture was extracted with diethyl ether (4 × 100 mL). The combined organic layers were washed with brine (100 mL) and water (100 mL) and dried over anhydrous sodium sulfate. The solvent was removed under reduced pressure, and the product was purified by column chromatography (hexane), yielding 0.64 g (32%) of **1** as a yellow solid whose characterization data are identical with that previously reported.[20]

4-(2-Pyridyl)-1*H*-1,2,3-triazol-1-ylferrocene (3). To a solution of **1** (0.15 g, 0.64 mmol) and 2-ethynylpyridine (**2**; 0.07 g, 0.7 mmol) in THF (9 mL) and water (3 mL) was added a solution of $CuSO_4 \cdot 5H_2O$ (0.159 g, 0.64 mmol) in water (4 mL). Then, a freshly prepared solution of sodium ascorbate (0.25 g, 1.27 mmol) in water (2 mL) was added dropwise, and the reaction mixture was stirred at room temperature overnight. After removal of THF under vacuum, dichloromethane (300 mL) and an aqueous solution of ammonia (15%) were added (100 mL). The mixture was stirred for 10 min to remove all of the copper(I) derivative trapped inside the product as $[Cu(NH_3)_6]^+$. The organic phase was washed with brine (100 mL) and then water (2 × 100 mL) and filtered through a Celite pad. The solvent was removed under vacuum, and the resulting product was crystallized from $CHCl_3$/*n*-hexane at −20 °C, yielding 0.17 g (81%) of **3** as a yellow solid. Mp: 252−254 °C. ^{1}H NMR (400 MHz, $CDCl_3$): δ 4.26 (s, 5H, Cp), 4.34 (st, 2H), 4.95 (st, 2H), 7.28 (dd, 1H, J = 6.8 and 5.2 Hz, H5 pyr), 7.83 (dt, 1H, J = 7.6 and 1.6 Hz, H4 pyr), 8.19 (d, 1H, J = 7.6 Hz, H3 pyr), 8.45 (s, 1H, CH triazole), 8.61 (d, 1H, J = 4.4 Hz, H6 pyr). ^{13}C NMR (150 MHz, $CDCl_3$): δ 62.0 (Fc-C_α), 66.8 (Fc-C_β), 70.2 (Cp), 93.6 (Fc-C_{ipso}), 120.4 (pyr C3), 121.1 (triazole CH), 123.0 (pyr C5), 137.0 (pyr C4), 148.3 (q), 149.4 (pyr C6), 150.1 (q). ESI-MS: *m*/*e* 353 (M^+ + 23), 331 (M^+ + 1). Anal. Calcd for $C_{17}H_{14}FeN_4$: C, 61.84; H, 4.27; N, 16.97. Found: C, 61.62; H, 4.45; N, 16.70.

1,1′-Bis[4-(2-pyridyl)-1*H*-1,2,3-triazol-1-yl]ferrocene (5). The procedure and reaction conditions used were exactly the same as thosedescribed above but using the following reagents: 1,1′-diazidoferrocene[21] (**4**; 0.5 g, 2.2 mmol) and **2** (0.5 g, 4.8 mmol) in THF (20 mL) and water (5 mL); a solution of $CuSO_4 \cdot 5H_2O$ (1.01 g, 4.4 mmol) in water (10 mL) and a solution of sodium ascorbate (1.75 g, 8.8 mmol) in water (5 mL). The resulting product was crystallized from $CHCl_3$/*n*-hexane at −20 °C, yielding **5** (68%) as a yellow solid. Mp: 248−250 °C (dec). ^{1}H NMR (400 MHz, $CDCl_3$): δ 4.37 (st, 2H), 5.03 (st, 2H), 7.6 (ddd, 1H, J = 7.6, 4.8, and 1.1 Hz, H5 pyr), 7.68 (td, 1H, J = 7.6 and 1.8 Hz, H4-pyr), 7.99 (dt, 1H, J = 7.6 and 1.8 Hz, H3 pyr), 8.19 (s, 1H, CH triazole), 8.53 (ddd, 1H, J = 4.8, 1.8, and 1.1 Hz, H6 pyr). ^{13}C NMR (100 MHz, $CDCl_3$): δ 63.5 (Fc-C_α), 69.0 (Fc-C_β), 95.0 (Fc-C_{ipso}), 120.4 (pyr C3), 120.9 (triazole CH), 123.0 (pyr C5), 136.9 (pyr C4), 148.5 (triazole q), 149.5 (pyr C6), 149.8 (q). ESI-MS: *m*/*e* 497 (M^+ + 23), 475 (M^+ + 1). Anal. Calcd for $C_{23}H_{19}FeN_8$: C, 59.63; H, 4.13; N, 24.19. Found: C, 59.81; H, 3.85; N, 24.43.

Scheme 1. Preparation of Triads 3 and 5[a]

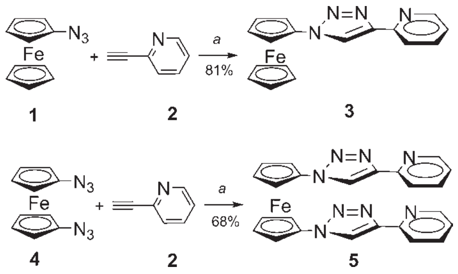

[a] Reagents: (*a*) $CuSO_4 \cdot 5H_2O$; sodium ascorbate; THF/H_2O, rt.

Preparation of the Complex $[3 \cdot Zn]^{2+}$. To a solution of **3** (0.3 mg, 1 μmol) in $CHCl_3$ (1 mL) was added a solution of $Zn(CF_3SO_3)_2$ (0.2 mg, 0.5 μmol) in CH_3CN (20 mL), and the solution was stirred for 30 min. The resulting precipitate was crystallized from CH_3CN/Et_2O (1:5) to give yellow needles suitable for X-ray diffraction analysis.

X-ray Structural Analysis. Suitable single crystals for X-ray diffraction were mounted in an inert oil on a glass fiber and transferred to a Bruker Smart APEX CCD diffractometer. Diffraction data were collected at 173 K using monochromated Mo Kα radiation (λ = 0.710 73 Å) in ω-scan mode. Data were corrected for absorption by using a multiscan method applied with the *SADABS*[22] program. The structures were solved by direct methods and all non-hydrogen atoms were refined anisotropically on F^2 using the program *SHELXL-97*.[23] All hydrogen atoms were initially located in a difference Fourier map and refined using a riding model. In all cases, final Fourier syntheses showed no significant residual electron density in chemically sensible positions.

Special Features and Exceptions: $[\mathbf{3}_2 \cdot Zn]^{2+}$. The cyclopentadienyl (Cp) C6 ring of the ferrocenyl moiety is disordered over two positions of approximately equal occupancy. The disordered carbon atoms were refined isotropically.

Computational Details. Quantum chemical calculations were performed with the *ORCA* electronic structure program package.[24] All geometry optimizations were run with tight convergence criteria[25] and without symmetry restrictions, first at the B3LYP[26] level using the new efficient *RIJCOSX* algorithm[27] and the def2-SVP[28] basis set and thereafter refined with the def2-TZVPP basis set.[29] For lead atoms, the [SD(60,MDF)] effective core potential[30] (ECP) was used. From these gas-phase-optimized geometries, all reported data were obtained by means of single-point calculations, at the same level of theory but using the more extensive def2-TZVPP basis set.[31] Reported energies are uncorrected for the zero-point vibrational energy. The topological analysis of the electronic charge density was conducted using the *AIM2000* software[32] and the wave functions generated at B3LYP/def2-TZVPP with the *Gaussian09* software package.[33] Wiberg's bond indices (WBI)[34] were calculated with the natural bond orbital (NBO) population analysis.[35] $\mathbf{3}_2Ni(ClO_4)_2$, $[\mathbf{5} \cdot Ni(ClO_4)_2]_2$, and $\mathbf{3} \cdot Pb(ClO_4)_2(MeCN)_2$ were generated with VMD.[36]

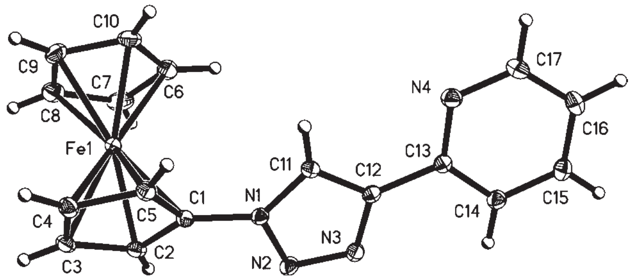

Figure 1. Molecular structure of **3**. Thermal ellipsoids are drawn at the 50% probability level. Selected bond lengths (Å) and angles (deg): Fe1−C1, 2.0314(12); N1−C1, 1.4164(16); N3−C12, 1.3634(16); N4−C13, 1.3471(16); C12−C13, 1.4669(17); N1−C1−Fe1, 127.41(9); N3−C12−C13, 122.10(11); N4−C13−C12, 116.05(11).

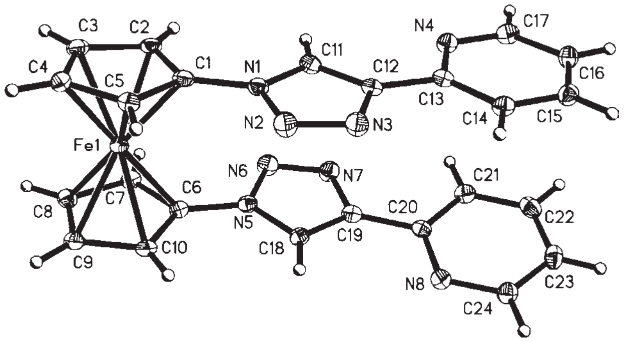

Figure 2. Thermal ellipsoid representation plot (50% probability) of compound **5**. Selected bond lengths (Å) and angles (deg): Fe1−C1, 2.031(2); Fe1−C6, 2.037(2); N1−C1, 1.416(3); N3−C12, 1.364(3); N4−C13, 1.348(3); N5−C6, 1.413(3); C12−C13, 1.468(3); C19−C20; 1.461(3); N1−C1−Fe1, 126.86(17); N5−C6−Fe1, 126.58(17); N3−C12−C13, 122.0(2); N4−C13−C12, 115.8(2); N7−C19−C20, 121.8(2); N8−C20−C19, 116.5(2).

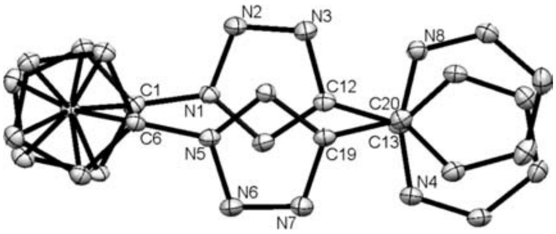

Figure 3. Partial overlap of the triazole and pyridine rings in the crystal structure of **5**. Hydrogen atoms have been omitted for clarity.

■ RESULTS AND DISCUSSION

Synthesis. The general strategy used for the synthesis of both **3** and **5** ferrocenyltriazole derivatives is based on the regioselective CuAAC of terminal alkynes and organic azides and is summarized in Scheme 1.

The synthesis of **3** starts with the preparation of azidoferrocene **1**, by using an improved method consisting in the initial metalation of ferrocene with the system ^{t}BuLi/K^{t}BuO followed by azidation with trisylazide (2,4,6-triisopropylbenzenesulfonylazide).[20] The synthesis of **5** requires the use of **4**[21] readily prepared from 1,1′-dilithioferrocene and the above-mentioned strong azide-transfer agent trisylazide. Compounds **1** and **4** undergo the "click reaction" with **2** to afford the triads **3** and **5** in 81% and 68% yield, respectively. Copper(I) and oxidized copper(II) species in the reaction mixture can be easily separated by treatment with aqueous ammonia during the workup and subsequent silica column chromatography.

The structures of compounds **3** and **5** were confirmed by means of standard spectroscopic techniques (^{1}H and ^{13}C NMR), electrospray ionization mass spectrometry (ESI-MS), and elemental analyses, with all data being in agreement with the proposed structures, which were finally established by X-ray diffraction analysis. A summary of the crystal data and details of data collection and refinement for **3** and **5** are summarized in Table S1 in the Supporting Information.

Compound **3** crystallizes from CD_2Cl_2 as a yellow prism in the monoclinic space group *P*21/*n*. Figure 1 shows the molecular structure of **3**, together with selected bond lengths and angles. The two Cp rings of the ferrocenyl moiety are perfectly planar. The Cp rings are arranged in a completely eclipsed conformation [the average torsion angle C1−centroid $(Cp)_1$−centroid $(Cp)_2$−C6 is 0.80°] and have an almost parallel orientation with a tilt angle of 1.3°. The organic ligand attached to the ferrocenyl moiety is almost planar (the deviation from the main plane is 0.0529 Å) and is rotated respect with to the Cp rings, with the angles between mean planes being 32.4° (C1 ring) and 33.7° (C6 ring).

Regarding the crystal structure of **3**, molecules are interlinked by intermolecular C5−H5···N2 hydrogen bonds (Table S2 in the Supporting Information), forming chains along the *a* axis. Molecules of adjacent chains stack together through $\pi\cdots\pi$ interactions between their parallel triazole and pyridine rings, resulting in the formation of ribbons along the cited axis. The ligands do not overlap completely, with the angle centroid $(pyridine)_1$-centroid $(triazole)_1$-centroid $(pyridine)_2$ being 76.2°, and the distance between ligands is 3.524 Å. The stacked molecules are further arranged, forming a sort of sheets parallel to (101) and perpendicular to the hydrogen-bonding network. In each sheet, the stacked molecules are oriented in two different directions, with one direction being approximately perpendicular to the other direction (see Figures S1−S4 in the Supporting Information).

Compound **5** crystallizes from $CHCl_3$/*n*-hexane as a yellow plate in the monoclinic space group *P*21/*n*. The molecular structure of **5** is given in Figure 2, where selected bond lengths and angles are also collected.

In the ferrocenyl moiety, the Cp rings are perfectly planar and almost parallel, with the tilt angle being 4.2°. The Cp rings are twisted from the eclipsed conformation by 18.08°. The organic ligands attached to the Cp rings are planar, with the deviations from the main planes being 0.0124 Å (C1 ring) and 0.0629 Å (C6 ring). The ligands adopt an almost parallel disposition with respect to the other (the angle between main planes is 9.6°) but deviate slightly from complete overlap (Figure 3). The triazole rings deviate from staking by a torsion angle N1−centroid $(Cp)_1$−centroid $(Cp)_2$−N5 of 19.00°, which seems to be dominated by a maximum overlap of parallel pyridine rings (distance of the projected pyridine ring centroid into the parallel plane 3.386 Å) and not to the equivalent overlapping of triazole rings (distance of projected triazole ring centroid into the parallel plane 3.529 Å). In the crystal structure, molecules of **5** are linked by intermolecular C2−H2···N7 hydrogen bonds (Table S2 in the Supporting Information), giving dimers. Similarly to **3**, the molecules of **5** arrange, forming a sort of sheet parallel to (101) and perpendicular to the hydrogen-bonding network. In each

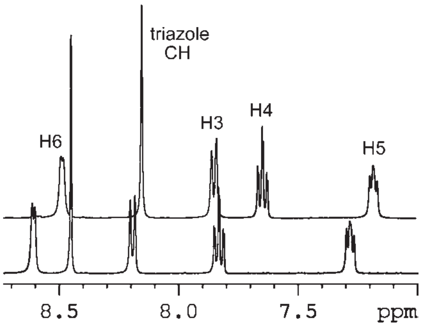

Figure 4. Aromatic region of the ^{1}H NMR spectra of compounds **3** (down) and **5** (up) carried out in CD_2Cl_2.

sheet, the molecules are oriented in two different directions, with one direction being approximately perpendicular to the other direction. The hydrogen-bonded dimers are formed between molecules of adjacent sheets (see Figures S5−S7 in the Supporting Information).

The common characteristic features observed in the ^{1}H NMR spectra of **3** and **5** are the presence of the typical pattern corresponding to the 2-substituted pyridine ring and the triazolyl proton signal. In addition, compound **3** also shows a singlet at δ 4.26, corresponding to the protons within the unsubstituted Cp ring of the ferrocene unit, while those present in the substituted Cp ring appear as two pseudotriplets located downfield at δ 4.95 for the H_α protons and at δ 4.34 for the H_β protons within the monosubstituted Cp ring. The ^{1}H NMR spectrum of **5** exhibits two characteristic pseudotriplets at δ 5.03 and 4.37 for two pairs of nonequivalent H_α and H_β protons present in the 1,1′-disubstituted ferrocene moiety.

Taking a closer look at the ^{1}H NMR of compounds **3** and **5**, almost identical chemical shifts of the signals assigned to the H_α and H_β protons present in both derivatives were observed. However, the signals corresponding to the pyridyl and triazolyl moieties are significantly shielded in **5** with reference to **3** (Figures 4 and S8 in the Supporting Information). The shielding is strongest for triazole CH ($\Delta\delta = 0.30$ ppm) and for pyridine H3 ($\Delta\delta = 0.34$ ppm) and H4 ($\Delta\delta = 0.19$ ppm), while the shielding of pyridine H5 ($\Delta\delta = 0.10$ ppm) and H6 ($\Delta\delta = 0.12$ ppm) is considerably less.

Because it is well-established that π-stacking interactions between aromatic rings affect the shielding of the protons due to anisotropy of the ring current effect,[37] the differences in chemical shifts observed between **3** and **5** could be associated with the different types of π-stacking interactions observed between the triazole−pyridine moieties existing in both ligands, as has already been demonstrated by a comparison of the single-crystal X-ray analysis of **3** and **5** shown previously. This π-stacking phenomenon has also been found in some other 1,1′-bis(azaaryl)-substituted ferrocenes.[38]

Cation Binding Studies. The redox chemistry of compounds **3** and **5** was investigated by CV, linear sweep voltammetry (LSV), and OSWV in a CH_3CN solution containing 0.1 M $TBAPF_6$ as the supporting electrolyte. Each receptor exhibited in the range 0−1.1 V a reversible one-electron redox wave, typical of a ferrocene derivative, at the half-wave potential value of $E_{1/2} = 0.714$ V and $E_{1/2} = 0.881$ V versus DMFc, for **3** and **5**, respectively (Figure S9 in the Supporting Information). The criteria applied for reversibility were a separation of ≈60 mV between cathodic and anodic peaks, a ratio of 1.0 ± 0.1 for the intensities of the cathodic and anodic currents I_c/I_a, and no shift of the half-wave potentials with varying scan rates. Likewise, OSWV also exhibits oxidation peaks at the same potentials as those observed in the corresponding CV.

Table 1. Electrochemical Data of Receptors 3 and 5 and Their Metal Complexes

compound	$E_{1/2}$[a]	$\Delta E_{1/2}$[b]	BEF[c]
3	714		
$[\mathbf{3}\cdot Ni]^{2+}$	805	91	35
$[\mathbf{3}\cdot Zn]^{2+}$	802	88	31
$[\mathbf{3}\cdot Cd]^{2+}$	784	70	15
$[\mathbf{3}\cdot Hg]^{2+}$	826	112	78
$[\mathbf{3}\cdot Pb]^{2+}$	844	130	158
5	881		
$[\mathbf{5}\cdot Ni]^{2+}$	1048	167	666
$[\mathbf{5}\cdot Zn]^{2+}$	1095	214	4147
$[\mathbf{5}\cdot Cd]^{2+}$	1049	168	692
$[\mathbf{5}\cdot Hg]^{2+}$	1066	185	1341
$[\mathbf{5}\cdot Pb]^{2+}$	1048	167	666

[a] In mV. [b] $\Delta E = E_{1/2}(\text{complex}) - E_{1/2}(\text{free receptor})$, in mV. [c] See ref 42.

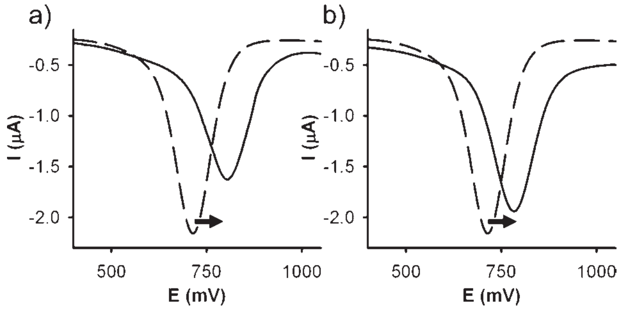

Figure 5. Evolution of the OSWV of **3** (dashed lines) (10^{-4} M in CH_3CN) scanned at 0.1 V/s with $[n\text{-}Bu_4N]PF_6$ as the supporting electrolyte upon the addition of 0.5 equiv of (a) Zn^{2+} and (b) Cd^{2+} metal cations (solid lines). Arrows indicate the total anodic shift promoted by the corresponding metal cation.

One important incentive for preparing these mono- and disubstituted heteroarylferrocene derivatives was to investigate their binding ability toward various metal cations such as Li^+, Na^+, K^+, Ca^{2+}, Mg^{2+}, Cu^{2+}, Ni^{2+}, Zn^{2+}, Cd^{2+}, Hg^{2+}, and Pb^{2+} as their triflates or perchlorate salts[39] (***Warning!*** *Perchlorate salts are hazardous because of the possibility of explosion; only small amounts of this material should be handled and with great caution*). Titration studies were carried out by using LSV and OSWV.[40] Thus, the addition of the above-mentioned set of metal cations to an electrochemical solution of receptor **3** ($c = 10^{-4}$ M) in CH_3CN containing $TBAPF_6$ (0.1 M) as the supporting electrolyte demonstrates that while the addition of Ni^{2+}, Zn^{2+}, Cd^{2+}, Hg^{2+}, and Pb^{2+} ions promotes remarkable responses, the addition of Li^+, Na^+, K^+, Ca^{2+}, and Mg^{2+} metal ions had no effect either on the LSV or on the CV or OSWV of this receptor, even when present in large excess. The results obtained upon the stepwise addition of substoichiometric amounts of those metal cations revealed the appearance, in the OSWV, of a new oxidation peak at more positive potentials associated with the formation of complexed species (Table 1). The current intensity of this new peak increases until 0.5 equiv of the guest cation is added. At this point,

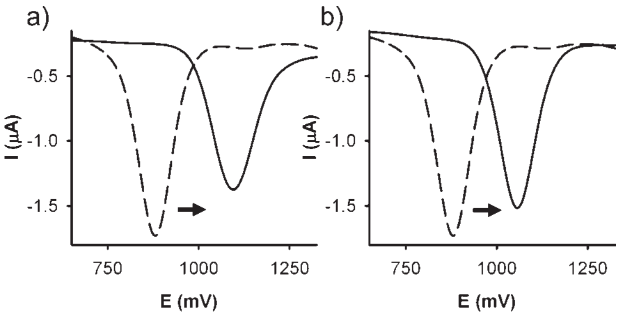

Figure 6. Evolution of the OSWV of **5** (dashed lines) (10^{-4} M in CH_3CN) scanned at 0.1 V/s with $[n\text{-}Bu_4N]PF_6$ as the supporting electrolyte, upon the addition of 1 equiv of (a) Zn^{2+} and (b) Cd^{2+} metal cations (solid lines). Arrows indicate the total anodic shift promoted by the corresponding metal cation.

the peak corresponding to the uncomplexed receptor **3** disappears (Figures 5 and S10−S14 in the Supporting Information).

The results obtained upon the stepwise addition of substoichiometric amounts of these metal cations to receptor **3** revealed a typical "two-wave behavior",[41] with the appearance of a second wave at a more positive potential, together with that corresponding to the free receptor, which is due to the cation-complexed species. In general, for receptor−cation systems exhibiting "two-wave behavior", both half-wave potentials can be obtained from the voltammetric data because both redox couples are simultaneously detected and then the binding enhancement factors (BEFs)[42] can be calculated (Table 1). This factor indicates the magnitude by which complexation in the oxidized form of the receptor is more difficult than that in the reduced one.

The positive potential shift observed for the Fe^{II}/Fe^{III} redox wave upon complexation by these cations can be due to the electrostatic repulsion effect between the bound metal cation and the electrogenerated positive charge on the oxidized ferrocenyl subunit. This leads to a decrease of the association constant with the oxidized ligand and to destabilization of the complex. Thus, $\Delta E_{1/2}$ reflects the balance of the interaction of the metal cation between the neutral and oxidized charged ligand.

Similar behavior was observed when receptor **5** was used (Table 1 and Figures 6 and S15−S19 in the Supporting Information). We, nevertheless, note that, in this case, the loss of the oxidation wave associated with the ferrocene moiety in the free receptor occurs when 1 equiv of the metal cation is added. In addition, the ΔE values found for receptor **5** (167−214 mV) are remarkably higher than those found for receptor **3** (70−130 mV) for the same cations.

A special behavior is observed upon the addition of Cu^{2+} to the CH_3CN solution of these ligands because Cu^{2+} behaves as an oxidizing agent toward ferrocene[43] with its concomitant reduction to Cu^+. In fact, LSV studies carried out upon the addition of Cu^{2+} to several types of ferrocenyl receptors have clearly demonstrated that Cu^{2+} promoted oxidation of the ferrocene unit, giving rise to a significant shift of the sigmoidal voltammetric wave toward cathodic currents.[44] However, similar LSV experiments carried out by using receptors **3** and **5** in the presence of this metal cation demonstrate that as oxidation of the receptors by the Cu^{2+} cation is taking place, the chemically generated Cu^+ is then complexed by the triazole−pyridine substituent. This behavior is reflected in the corresponding LSV obtained, which clearly shows the development of both processes: oxidation and complexation of Cu^+ resulting from the reduction of Cu^{2+} by the ferrocenyl receptor (Figure S20 in the Supporting Information).

One of the most important attributes of receptors **3** and **5** is the presence of one ferrocene moiety in the proximity of the cation binding nitrogen atoms. Previous studies on ferrocene-based ligands have shown that their characteristic low-energy (LE) bands are perturbed by complexation.[45] Therefore, the metal coordination properties of ligands **3** and **5** toward the above-mentioned set of metal cations were also evaluated by UV−vis spectroscopy (Table 2).

The UV−vis spectra of the free ligands **3** and **5** ($c = 1 \times 10^{-4}$ M and 5×10^{-5} M, respectively) in CH_3CN exhibited two main absorption bands at 240 and 283 nm with a shoulder band at 326 nm, which can safely be ascribed to a high-energy ligand-centered $\pi-\pi^*$ electronic transition. In addition, another weaker absorption is visible at around 435 nm, which can be assigned to another localized excitation with a lower energy produced either by two nearly degenerate transitions and Fe^{II} d−d transitions[46] or by a metal−ligand charge-transfer process ($d\pi-\pi^*$; LE band). This assignment is in agreement with the latest theoretical treatment (model III) reported by Barlow et al.[47] Such spectral characteristics confer a yellow color to these species.

Titration experiments in CH_3CN solutions of these ligands ($c = 1 \times 10^{-4}$ M for ligand **3** and 5×10^{-5} M for **5**) and the corresponding ions were performed and analyzed using the computer program *Specfit*.[48] It is worth mentioning that no changes at all were observed in the UV−vis spectra of compounds **3** and **5** in CH_3CN upon the addition of 1 equiv of Li^+, Na^+, K^+, Mg^{2+}, and Ca^{2+}. However, with the stepwise addition of increasing amounts of Ni^{2+}, Zn^{2+}, Cd^{2+}, Hg^{2+}, and Pb^{2+} metal ions, the absorption band centered at around 240 nm slightly decreased and that appearing at 283 nm increased in intensity until the appropriate amount of the corresponding cations was added. Simultaneously, two new absorption bands at around 335 and 440 nm were gradually developed, while the shoulder exhibited at 326 nm in the free ligands disappeared (Figures 7 and 8 and S21 and S22 in the Supporting Information). Meanwhile, these changes promoted a very slight change of color in the corresponding solutions.

Job's plot analysis[49] of the UV−vis titration spectra carried out by using ligand **3** show that Ni^{2+}, Zn^{2+}, Cd^{2+}, and Hg^{2+} metal cations induce the formation of complexes in a 2:1 (ligand/cation) stoichiometry, while in the case of Pb^{2+}, the formation of the corresponding complex takes place in a 1:1 stoichiometry. On the other hand, the stoichiometries of the complexes formed with ligand **5** are 1:1 (ligand/cation). The observation of isosbestic points during the titration experiments clearly indicates that clean complexation reactions take place. On the basis of the stoichiometries observed and the absorption titration data, the stability constants displayed in Table 2 were calculated.[48]

The stoichiometries proposed from absorption data have been further confirmed by ESI-MS in the presence of the metal cations. The ESI-MS spectra of receptor **3** in the presence of Ni^{2+}, Zn^{2+}, Cd^{2+}, and Hg^{2+} metal cations show the peaks at values of m/z corresponding to the complex 2:1, and the relative abundance of their isotopic clusters was in good agreement with the simulated spectrum of the corresponding $[\mathbf{3}_2\cdot M]^{2+}$ complex (Figures S24−S31 in the Supporting Information). Likewise, the formation of the 1:1 complex was also proven by the presence of the molecular ion peak at m/z 538 corresponding to the formation of the $[\mathbf{3}\cdot Pb]^{2+}$ species (Figures S32 and S33 in the

Table 2. UV−Vis Data of Receptors 3 and 5 in the Presence of Metal Cations

compound	UV−vis: λ_{max} ($10^{-3}\varepsilon$)[a]	IP[b]	β[c]
3	242 (20.67), 283 (13.29), 326 (2.17) sh, 436 (0.35)		
$[\mathbf{3}\cdot Ni]^{2+}$	235 (20.18), 283 (18.38), 335 (1.94), 440 (0.5)	236, 264, 300, 330	$\beta_1 = 6.21 \times 10^6$ (±2) $\beta_2 = 1.82 \times 10^{12}$ (±4)
$[\mathbf{3}\cdot Zn]^{2+}$	235 (20.43), 283 (18.66), 334 (1.89), 441 (0.49)	266, 300	$\beta_1 = 1.67 \times 10^6$ (±1) $\beta_2 = 2.01 \times 10^{11}$ (±2)
$[\mathbf{3}\cdot Cd]^{2+}$	237 (20.28), 282 (20.57), 331 (1.9), 441 (0.49)	262, 301, 336	$\beta_1 = 7.24 \times 10^5$ (±2) $\beta_2 = 3.38 \times 10^8$ (±2)
$[\mathbf{3}\cdot Hg]^{2+}$	237 (19.47), 285 (16.55), 344 (1.93), 441 (0.62)	219, 267, 331	$\beta_1 = 2.47 \times 10^5$ (±2) $\beta_2 = 6.48 \times 10^8$ (±2)
$[\mathbf{3}\cdot Pb]^{2+}$	238 (21.91), 283 (16.32), 346 (2.03) sh, 440 (0.6)	239, 266, 329	$\beta = 1.01 \times 10^5$ (±1)
5	240 (35.3), 283 (21.3), 326 (2.2) sh, 435 (0.5)		
$[\mathbf{5}\cdot Ni]^{2+}$	235 (34.3), 283 (30.0), 329 (3.7) sh, 440 (0.7)	261, 301	$\beta = 9.87 \times 10^5$ (±2)
$[\mathbf{5}\cdot Zn]^{2+}$	236 (32.4)282 (26.8), 337 (3.4) sh, 442 (0.7)	213, 262, 300, 331	$\beta = 7.99 \times 10^6$ (±3)
$[\mathbf{5}\cdot Cd]^{2+}$	236 (33.6), 280 (24.9), 334 (3.4) sh, 442 (0.6)	209, 258, 331	$\beta = 2.51 \times 10^6$ (±3)
$[\mathbf{5}\cdot Hg]^{2+}$	237 (29.0), 288 (24.9), 344 (3.6) sh, 441 (0.7) sh	222, 277	$\beta = 3.31 \times 10^6$ (±5)
$[\mathbf{5}\cdot Pb]^{2+}$	231 (38.0), 256 (27.7), 281 (20.2), 346 (2.9) sh, 445 (0.5)	253, 336	$\beta = 3.38 \times 10^6$ (±4)

[a] λ_{max} in nm; ε in $dm^3/(mol\ cm)$. [b] Isosbestic points in nm. [c] Complexation constants β and β_1 are given in M^{-1}, while β_2 is given in M^{-2}.

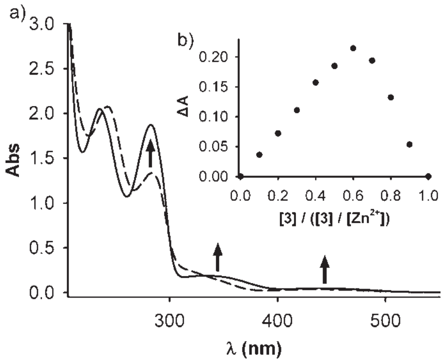

Figure 7. (a) Variation of the UV−vis in CH_3CN of compound **3** ($c = 1 \times 10^{-4}$ M) (dashed line) upon the addition of 0.5 equiv of Zn^{2+} metal cation. Arrows indicate the absorptions that increase during this experiment. (b) Job's plot evaluated from the absorption spectra of the titration solution exhibiting the formation of a 2:1 (ligand/cation) complex ($\Delta A = A_{obsd} - A_{host} - A_{guest}$; all measured at λ = 283 nm).

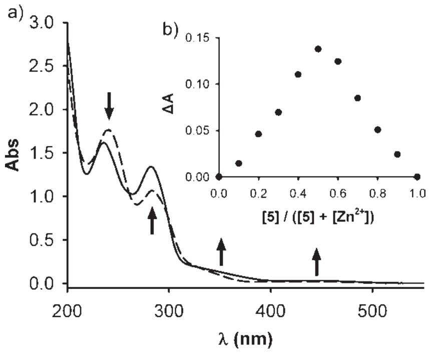

Figure 8. (a) Variation of the UV−vis in CH_3CN of compound **5** ($c = 5 \times 10^{-5}$ M) (dashed line) upon the addition of 0.5 equiv of Zn^{2+} metal cation. Arrows indicate the absorptions that increase or decrease during this experiment. (b) Job's plot evaluated from the absorption spectra of the titration solution exhibiting the formation of a 1:1 (ligand/cation) complex ($\Delta A = A_{obsd} - A_{host} - A_{guest}$; all measured at λ = 283 nm).

Supporting Information). Moreover, the ESI-MS spectra obtained by the addition of those metal cations to the two-armed receptor **5** show molecular ion peaks, indicating that the formation of the corresponding $[\mathbf{5}\cdot M]^{2+}$ complexes takes place (Figures S35−S44 in the Supporting Information).

The binding properties of receptors **3** and **5** with Ni^{2+}, Zn^{2+}, Cd^{2+}, Hg^{2+}, and Pb^{2+} metal ions were also evaluated by ^1H NMR studies in CD_3CN solutions, with the most significant features observed being the following: (i) both receptors gave rise to paramagnetic species when the Ni^{2+} metal cation was added; (ii) the hydrogen atom within the triazole ring in **3** and **5** showed a significant downfield shift, demonstrating that this unit is involved in the ligand−cation binding event; (iii) downfield shifts were also observed for the pyridine ring hydrogen atoms H4 and H5, which could also be related to the participation of the pyridine nitrogen atom in the binding process; (iv) the cyclopentadieneyl ring protons were almost unchanged in both ligands (Figures 9 and S45−S52 and Table S11 in the Supporting Information).

To gain insight into the structure of the complexes formed, density functional theory (DFT) calculations and X-ray analysis were carried out. Unfortunately, the only suitable crystals for a X-ray diffraction study were obtained by crystallization of the complex $[\mathbf{3}_2\cdot Zn]^{2+}$ from acetonitrile/diethyl ether (1:5), which crystallizes as yellow needles in the monoclinic space group *P*21/*n*. A summary of the crystal data and details of data collection and refinement are summarized in Table S12 in the Supporting Information. Figure 10 shows the molecular structure of $[\mathbf{3}_2\cdot Zn]^{2+}$ together with selected bond lengths and angles. The asymmetric unit cell consists of half of a zinc(II) complex situated on an inversion center and one molecule of chloroform in a general position. Similarly to **3**, the organic ligand attached to the ferrocenyl moiety is almost planar and rotated with respect to the Cp rings by an average angle of 21°. The two Cp rings are eclipsed and almost parallel, with the tilt angle being 2.9°. The organic ligands of two molecules coordinate to the Zn^{II} ion via four nitrogen atoms, with the ligands acting as bidentate ligands. The atoms involved in the coordination are the triazole nitrogen

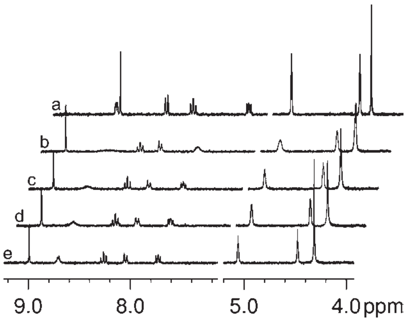

Figure 9. Evolution of the ^{1}H NMR spectra of **3** in CD$_3$CN upon the addition of the Zn^{2+} metal cation from (a) 0 to (e) 0.8 equiv.

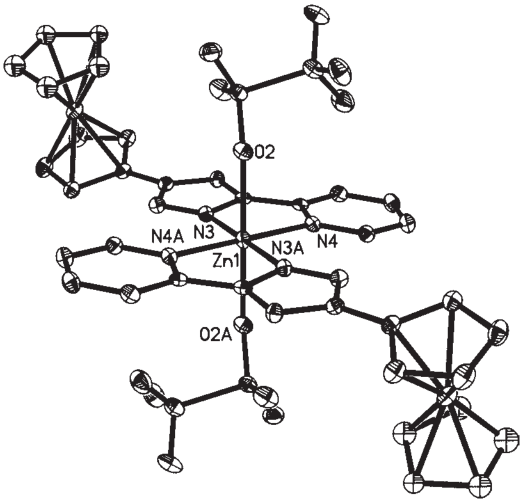

Figure 10. Thermal ellipsoid representation plot (50% probability) of complex $[\mathbf{3}_2\cdot\text{Zn}]^{2+}$. Selected bond lengths (Å) and angles (deg): Zn1−N3, 2.127(2); Zn1−N3A, 2.127(2); Zn1−N4, 2.096(2); Zn1−N4A, 2.096(2); Zn1−O2, 2.1940(19); Zn1−O2A, 2.1939(19); N4−Zn1−N4A, 180.0; N4−Zn1−N3A, 101.02 (8), N4A−Zn1−N3A 78.99 (8); N4−Zn1−N3, 78.99(8), N4A−Zn1−N3 101.01(8); N3A−Zn1−N3, 180.0; N4−Zn1−O2A, 87.47(8); N4A−Zn1−O2A, 92.53(8); N3A−Zn1-O2A, 92.44(8); N3−Zn1−O2A, 87.56(8); N4−Zn1−O2, 92.53(8); N4A−Zn1−O2, 87.47(8); N3A−Zn1−O2, 87.56(8); N3−Zn1−O2, 92.44(8); O2A−Zn1−O2, 180.0.

N3 and the pyridine nitrogen N4. The Zn^{II} ion is six-coordinated, resulting in a slightly distorted octahedral geometry, with the nitrogen atoms N3, N3A, N4, and N4A forming a square-planar arrangement and two trans-oriented triflate anions completing the coordination sphere. The Zn−N distances are 2.127(2) and 2.096(2) Å, while the Zn−O distance is 2.194(2) Å. In sharp contrast to Mg^{2+}, which is usually octahedrally coordinated both in aqueous solution and in proteins,[50] it is worth mentioning that Zn^{2+}, being also divalent and with an ionic radius (0.74 Å) similar to that of Mg^{2+} (0.65 Å), is flexible with respect to the number of ligands it can adopt in its first-coordination shell. Although in aqueous solution Zn^{2+} is coordinated to six water molecules,[51] in both zinc-finger proteins and enzymes, zinc is usually *tetrahedrally* coordinated, but in some catalytic binding sites, it is found pentacoordinated and, rarely, hexacoordinated.[52] In connection to this, Pavlov et al.[53] have computationally examined big clusters with a rather complete second coordination layer and found that the tetrahedral $\{[\text{Zn(H}_2\text{O)}_4]\cdot(\text{H}_2\text{O})_8\}^{2+}$ complex is more stable (by 5.6 kcal/mol) than the octahedral $\{[\text{Zn(H}_2\text{O)}_6]\cdot(\text{H}_2\text{O})_6\}^{2+}$ cluster.

Chart 1. Model Ligands

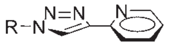

6 R: CH$_3$
7 R: 4-CH$_3$O-C$_6$H$_4$

In the crystal, complexes of $[\mathbf{3}_2\cdot\text{Zn}]^{2+}$ are linked by intermolecular C11−H11···O1 hydrogen bonds, with each complex participating in a total of four of these C−H···O hydrogen bonds. The result is the formation of ribbons parallel to (001). The ribbons are connected through C16−H16···F1 hydrogen bonds, with each complex participating again in a total of four of these C−H···F hydrogen bonds. Molecules of chloroform retained in the lattice also contribute to the three-dimensional hydrogen-bonding network of the crystal structure acting as a bridge connecting adjacent complexes through C8−H8···Cl1 and C22−H22···O1 hydrogen bonds (see Figures S54−S56 and Tables S13−S17 in the Supporting Information). Complexes are further arranged in a sort of sheet parallel to the *ab* plane. In each sheet, all of the complexes are oriented in the same direction, with the main plane of the organic ligands forming an angle of approximately 27.7° with respect to the sheet. Complexes belonging to adjacent sheets orientate differently, forming an angle of approximately 152.5° with respect to the sheet. The angle formed by the main planes of the organic ligands of adjacent sheets is of approximately 51.5°.

Further insight regarding the binding and stoichiometries in the above-mentioned complexes has been extracted from DFT calculations (see the Computational Details section). First of all, we selected a simplified model for ligand **3** by just substituting the ferrocenyl group by an electronically similar methyl (**6**) or even roughly equivalent *p*-methoxyphenyl (**7**) substituents (Chart 1). Both the actual (**3**) and the model free ligands (**6** and **7**) show a preferred most stable *anti-periplanar* conformation with respect to the relative positions of the closest nitrogen atoms in the pyridine and triazole rings. Chelate formation requires its preorganization in the *syn-periplanar* conformation, which is ca. 6 kcal/mol less stable (6.19, 6.07, and 6.04 kcal/mol for **6**, **7**, and **3**, respectively).

Complexes of these ligands with the Ni^{2+} cation were studied computationally in order to evaluate the origin of the observed magnetic behavior. In the case of model ligands **6** and **7**, the most stable complexes were found to be those with a head-to-tail arrangement slightly distorted from the square-planar geometry around the metal and having C_2 overall symmetry (*ht*-C_2). The second most stable isomers (by 2.98 and 0.62 kcal/mol for **6** and **7**, respectively) were those with perfect square-planar coordination around Ni^{2+} and C_i ovearll symmetry (*ht*-C_i), which constitutes the absolute minimum energy complex derived from the actual ligand **3** ($\Delta E = -0.27$ kcal/mol in relation to *ht*-C_2). All three most stable complexes feature a stronger bond between the N3 atom at the triazole ring (N3$_t$) and nickel ($d_{\text{Ni-N}} = 1.917-1.925$ Å; WBI = 0.468−0.471) in comparison to the other bond formed with the pyridine nitrogen (N$_p$) atom ($d_{\text{Ni-N}} = 1.973-1.991$ Å; WBI[34] = 0.450−0.458). This tendency is also observed using other bond strength parameters such as the Löwdin bond orders[54] (LBO 0.745−0.770 and 0.673−0.722 for Ni−N3$_t$ and Ni−N$_p$, respectively) and the electron density at bond critical points derived from the Bader's atoms-in-molecules

Chart 2. $L_2Ni(ClO_4)_2$ Stereoisomers and Relative Energies (kcal/mol) for the Simplest L: 6 Case

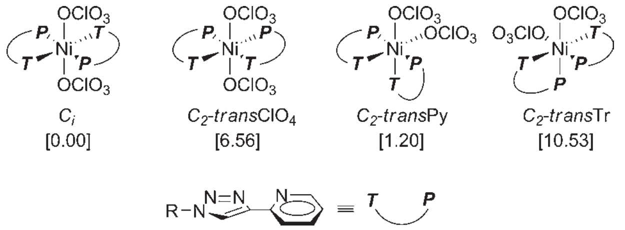

(AIM) methodology[55] [$\rho(\mathbf{r}_c) \times 10^2 = 10.31-10.55$ and $9.15-9.57\ e/a_0^3$ for Ni–N3$_t$ and Ni–N$_p$, respectively]. A pair of hydrogen bridge bonds between the N2$_t$ atom and H6$_p$ in different ligands [$d_{N\cdots H} = 2.057-2.207$ Å; WBI = 0.011–0.020; LBO 0.066–0.102; $\rho(\mathbf{r}_c) \times 10^2 = 1.76-2.41\ e/a_0^3$] contribute to an extra stabilization of the aforementioned *ht* complexes in relation to a third type of C_2-symmetric head-to-head (*hh*-C_2) less stable complexes (ΔE_{rel} = 2.61, 6.15, and 5.88 kcal/mol for complexes derived from **6**, **7**, and **3**, respectively). In the later *hh*-C_2 complexes, the close proximity of electron lone pairs at N2$_t$ and of H6$_p$ atoms belonging to different ligands forces a tetrahedral distortion in the coordination sphere around the Ni^{2+} atom (angles between chelate rings of 24.5°, 25.6°, and 22.7° for complexes derived from **6**, **7**, and **3**, respectively). Nevertheless, the occurrence of any of these above-mentioned L_2Ni^{2+}-type (L = **6**, **7**, and **3**) complexes in the reaction of **3** with Ni^{2+} salts can be ruled out on the basis of their strictly closed-shell electron configuration maintained even for those tetrahedrally distorted.

Moreover, the unusually high tendency displayed by ligand **3** to favor hexacoordination in other divalent cations such as Zn^{2+} (Figure 10) and the fact that the conductivity of an acetonitrile solution of $Ni(ClO_4)_2$ decreases upon complexation with **3**, indicating that the ionicity did not increase once the complex was formed,[56] prompted us to consider the coordinative role of the perchlorate counteranions in the case of Ni^{2+}. It is known that whereas Ni^{2+} tends to form low-spin ($S = 0$, i.e., diamagnetic) complexes, octahedral complexes are nearly always high-spin ($S = 1$, i.e., paramagnetic) and square-pyramidal (pentacoordinated) complexes are either high or low spin depending on the nature of the ligands. This concept has been used for the design of molecular spin switches based on Ni^{2+}, which are bistable in solution.[57] On the basis of these observations, we have computed four possible diastereomers of hexacoordinated $L_2Ni(ClO_4)_2$ complexes for the case of the simplest ligand **6** (Chart 2). In all cases, the triplet electronic states were the most stable ones (see below). The two first stereoisomers, named C_i and C_2 *trans*-ClO$_4$, are derived from the *ht*-C_i and *hh*-C_2 L_2Ni^{2+} complexes by the addition of perchlorate ligands at apical (i.e., trans to each other) positions. In the latter case, the steric bulk of the equatorial L chelate ligands promotes a distortion from the planarity that reduces the symmetry to C_2 (no symmetry planes are present), yielding a pair of C_2*trans*-ClO$_4$ enantiomers that are remarkably less stable than the absolute minimum energy C_i isomer. Two other diastereomeric pairs of C_2-symmetric enantiomers are obtained on locating the two chelate ligands in the orthogonal planes (perchlorate ligands in relative cis positions to each other), the most stable of which is the one placing the pyridine nitrogen atoms in relative trans positions. The occurrence of pentacoordinated species was ruled out because of the computed instability of a hypothetical square-pyramidal triplet species $[\mathbf{6}_2Ni(ClO_4)]^+ClO_4^-$ derived from the hexacoordinated C_i isomer by elongation of one of the Ni–OClO$_3$ bonds, which spontaneously reverts back to the octahedral species $[\mathbf{6}_2Ni(ClO_4)_2]$ following a barrierless process. Also, taking the most stable C_i triplet species $[\mathbf{6}_2Ni(ClO_4)_2]$ as a reference, the singlet state (see the Supporting Information) was found to be 15.04 kcal/mol less stable and features elongated (weaker) distal nickel–perchlorate bonds together with shorter (stronger) equatorial Ni–N bonds.[58]

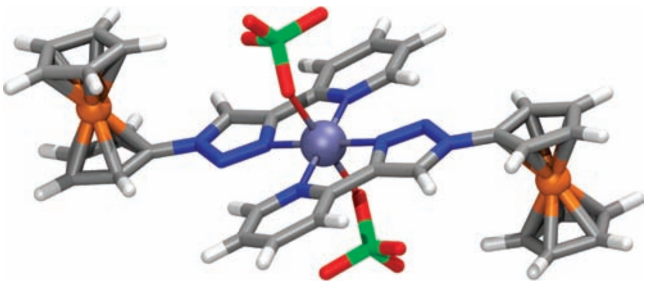

Figure 11. Calculated (RIJCOSX-B3LYP/def2-TZVP) most stable (C_i) structure for complex $\mathbf{3}_2Ni(ClO_4)_2$.

For the case of the two larger chelating L ligands **7** and **3**, only the most stable C_i stereoisomers were computed. Again, bonding to N3$_t$ is much stronger than that to N$_p$ and features a strong Ni–O bond slightly bent toward one of the pyridine rings.[59] Also, a pair of interligand N2$_t\cdots$H6$_p$ hydrogen bonds [$d_{N\cdots H}$ = 2.418–2.436 Å; WBI = 0.006–0.008; LBO < 0.01; $\rho(\mathbf{r}_c) \times 10^2 = 1.00-1.04\ e/a_0^3$] help to keep a robust coordination sphere around the central Ni^{2+} ion (Figure 11). The two unpaired electrons are almost entirely kept at the nickel atom [Mulliken spin density = 1.684–1.687 au (Figure S57 in the Supporting Information)].

When the receptor used for the reaction with Ni^{2+} salts is the bis-heterocyclic side-armed ferrocene derivative **5**, the simplest $\mathbf{5}\cdot Ni(ClO_4)_2$ molecular formula directly derived from the experimentally inferred 1:1 ligand–metal ratio can be ruled out on the basis of geometrical considerations upon inspection of the different stereoisomeric possibilities shown for the single-armed model $\mathbf{3}_2Ni(ClO_4)_2$ (Chart 2). When bringing together both side arms around the ferrocene hinge in order to complex Ni^{2+}, the arrangements locating the triazole rings (directly connected to the ferrocene moiety) trans to each other (C_i and C_2 *trans*-Tr) are obviously not possible, whereas both other diastereomers (C_2 *trans*-ClO$_4$ and C_2 *trans*-Py) feature the triazole units cis to each other but too separated and divergently oriented, thus hampering their direct connection through a ferrocenyl bridge. The next simplest compatible molecular formula that could be envisaged is a dimer $[\mathbf{5}\cdot Ni(ClO_4)_2]_2$ with cis-oriented triazole units at every nickel center. We have explored the two possible stereoisomers having identical coordination environments around both nickel atoms and the most stable quintuplet electronic state. At a moderate computational level (RIJCOSX-B3LYP/def2-SVP), the most stable geometry was that displaying *trans*-Py arrangement without the overall symmetry (Figure S58 in the Supporting Information). The other diastereomer is only 0.68 kcal/mol less stable at this level of theory and shows *trans*-ClO$_4$ arrangement at every metal center and overall C_i symmetry. It is worth mentioning that this difference is much less than expected

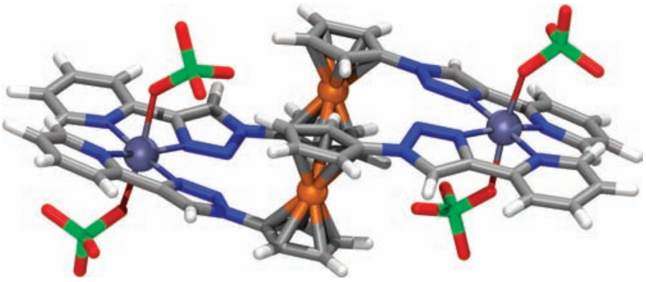

Figure 12. Calculated (RIJCOSX-B3LYP/def2-TZVP) C_i-symmetric (see the text) structure for complex $[\mathbf{5}\cdot Ni(ClO_4)_2]_2$.

according to the relative energies of the C_2 *trans*-ClO_4 and C_2 *trans*-Tr isomers in $\mathbf{3}_2Ni(ClO_4)_2$ (Chart 2). For the sake of simplicity, only the symmetric structure was further refined with the more extensive def2-TZVP basis set (Figure 12).[60] The most weakly bound perchlorate axial ligand at every nickel atom forms two hydrogen bonds with hydrogen atoms belonging to different ferrocene units [$d_{O\cdots H}$ = 2.481, 2.555 Å; WBI = 0.003, 0.003; LBO < 0.05; $\rho(\mathbf{r}_c) \times 10^2$ = 0.72, 0.62 e/a_0^3] that are slightly interpenetrated and kept close to a contact bonding [$d_{CpH\cdots HCp}$ = 2.759 Å; WBI < 0.001, LBO < 0.05; $\rho(\mathbf{r}_c) \times 10^2$ = 0.15 e/a_0^3; $d_{Fe\cdots Fe}$ = 7.359 Å].

Regarding the complexation of $Pb(ClO_4)_2$ by receptor **3**, the 1:1 ligand−metal ratio inferred by UV−vis titration experiments and the ESI-MS spectrum could be explained by the formation of a $\mathbf{3}\cdot Pb(ClO_4)_2(CH_3CN)_n$ complex, in analogy with previously reported examples.[61] The Pb^{2+} cation is surrounded by the two nitrogen-donor atoms at the chelating ligand **3**, with the $N3_t$ being more strongly bound, and four oxygen atoms belonging to two perchlorate ligands (Figure S59 in the Supporting Information).[62] The coordination sphere around the large metal ion is completed with two more weakly bound solvent (acetonitrile) nitrogen atoms.[63]

CONCLUSION

The triads ferrocene−triazole−pyridine **3** and **5** have been prepared from the appropriate azido ferrocene derivative **1** or **4** and **2** under "click" reaction conditions. In these structures, the presence of a nitrogen-rich cavity, suited for hosting cationic species, and a redox-active ferrocene unit are combined. Consequently, the binding abilities of these organometallic−organic hybrids toward divalent metal cations have been studied by using electrochemical, optical, and spectroscopic techniques.

Electrochemical studies showed that Zn^{2+}, Ni^{2+}, Cd^{2+}, Hg^{2+}, and Pb^{2+} induced a clear perturbation of the ferrocene/ferrocinium redox couple, which is anodically shifted by 70−130 mV for **3** and 167−214 mV for **5**. In addition, the LE bands of the absorption spectra of triads **3** and **5** are red-shifted ($\Delta\lambda$ = 5−10 nm) upon complexation with these metal cations. The ^1H NMR studies revealed that the hydrogen atom of the triazole ring as well as the H4 and H5 atoms of the pyridine ring are significantly downfield-shifted after complexation. These results are in good agreement with the cystal data of the $[\mathbf{3}_2\cdot Zn]^{2+}$ complex, which showed that the triad is acting as a bidentate ligand through the triazole N3 atom and the pyridine N4 atom.

ASSOCIATED CONTENT

Ⓢ Supporting Information. NMR spectra, X-ray crystallographic data for compounds **3**, **5**, and $[\mathbf{3}_2\cdot \mathbf{Zn}]^{2+}$ in CIF format, electrochemical, UV−vis, and ^1H NMR titration data, Job's plots, structures, energies, and Cartesian coordinates of all computed compounds. This material is available free of charge via the Internet at http://pubs.acs.org.

AUTHOR INFORMATION

Corresponding Author
*E-mail: pmolina@um.es (P.M.), atarraga@um.es (A.T.).

ACKNOWLEDGMENT

We gratefully acknowledge financial support from MICINN-Spain (Project CTQ2008-01402) and Fundación Séneca (Agencia de Ciencia y Tecnología de la Región de Murcia; Project 04509/GERM/06; Programa de Ayudas a Grupos de Excelencia de la Región de Murcia, Plan Regional de Ciencia y Tecnología 2007/2010). We also thank the Supercomputation Center at "Fundación Parque Científico de Murcia" for their technical support and the computational resources used in the supercomputer Ben-Arabí.

REFERENCES

(1) Huisgen, R.; Szeimies, G.; Möbius, L. *Chem. Ber.* **1967**, *100*, 2494–2507.

(2) (a) Rostovtsev, V.; Green, L. G.; Fokin, V. V.; Sharpless, K. B. *Angew. Chem., Int. Ed.* **2002**, *41*, 2596–2599. (b) Tornoe, C. V.; Christensen, C.; Medal, M. *J. Org. Chem.* **2002**, *67*, 3057–3064.

(3) Kolb, H. C.; Finn, M. G.; Sharpless, K. B. *Angew. Chem., Int. Ed.* **2001**, *40*, 2004–2021.

(4) Struthers, H.; Mindt, T. L.; Schibli, R. *Dalton Trans.* **2010**, *39*, 675–696.

(5) (a) Huang, S.; Clark, R. J.; Zhu, L. *Org. Lett.* **2007**, *9*, 4999–5002. (b) Schweinfurth, D.; Hardcastle, K. I.; Bunz, U. H. F. *Chem. Commun.* **2008**, 2203–2205. (c) Tamanini, E.; Katewa, A.; Sedger, L. M.; Todd, M. H.; Watkinson, M. *Inorg. Chem.* **2009**, *48*, 319–324. (d) Tamanini, E.; Rigby, S. E. J.; Motevalli, M.; Todd, M. H.; Watkinson, M. *Chem.—Eur. J.* **2009**, *15*, 3720–3728.

(6) (a) Li, Y.; Huffman, J. C.; Flood, A. H. *Chem. Commun.* **2007**, 2692–2694. (b) Meudtner, R. M.; Ostermeier, M.; Goddard, R.; Limberg, C.; Hecht, S. *Chem.—Eur. J.* **2007**, *13*, 9834–9840. (c) Fletcher, J. T.; Bumgarner, B. J.; Engels., N. D.; Skoglund, D. A. *Organometallics* **2008**, *27*, 5430–5433. (d) Schulze, B.; Friebe, C.; Hager, M. D.; Winter, A.; Hoogenboom, R.; Görls, H.; Schubert, U. S. *Dalton Trans.* **2009**, 787–794. (e) Happ, B.; Friebe, C.; Winter, A.; Hager, M. D.; Hoogenboom, R.; Schubert, U. S. *Chem.—Asian J.* **2009**, *4*, 154–163. (f) Happ, B.; Escudero, D.; Hager, M. D.; Friebe, C.; Winter, A.; Görls, H.; Altuntas, E.; González, L.; Schubert, U. S. *J. Org. Chem.* **2010**, *75*, 4025–4038.

(7) Bronisz, R. *Inorg. Chem.* **2005**, *44*, 4463–4465.

(8) (a) Haridas, V.; Lal, K.; Sharma, Y. K.; Upreti, S. *Org. Lett.* **2008**, *10*, 1645–1647. (b) Hua, Y.; Flood, A. H. *Chem. Soc. Rev.* **2010**, *39*, 1262–1271.

(9) Horne, W. S.; Yadav, M. K.; Scout, C. D.; Ghadiri, M. R. *J. Am. Chem. Soc.* **2004**, *126*, 15366–15367.

(10) Li., Y.; Flood, A. H. *Angew. Chem., Int. Ed.* **2008**, *47*, 2649–2652.

(11) (a) Juwarker, H.; Lenhardt, J. M.; Pham, D. M.; Craig, S. L. *Angew. Chem., Int. Ed.* **2008**, *47*, 3740–3743. (b) Meudtner, R. M.; Hecht, S. *Angew. Chem., Int. Ed.* **2008**, *47*, 4926–4930.

(12) Romero, T.; Caballero, A.; Tárraga, A.; Molina, P. *Org. Lett.* **2009**, *11*, 3466–3469.

(13) (a) Djeda, R.; Rapakousion, A.; Liang, L. Y.; Guidolin, N.; Ruiz, J.; Astruct, D. *Angew. Chem., Int. Ed.* **2010**, *49*, 8152–8156. (b) Ornelas, C.; Ruiz, J.; Astruct, D. *Organometallics* **2009**, *28*, 4431–4437. (c) Ornelas,

C.; Aranzaes, J. R.; Cloutet, E.; Alves, S.; Astruc, D. *Angew. Chem., Int. Ed.* **2007**, *46*, 872–877.

(14) (a) Lehn, J.-M. *Supramolecular Chemistry, Concepts and Perspectives*; Wiley-VCH: Weinheim, Germany, 1995. (b) Ward, M. D. *Annu. Rep. Prog. Chem., Sect. A* **2002**, *98*, 285–320.(c) Schubert, U. S.; Hofmeier, H.; Newkome, G. R. *Modern Terpyridine Chemistry*; Wiley-VCH: Weinheim, Germany, 2006. (d) Northrop, B. H.; Yang, H.-B.; Stang, P. *Chem. Commun.* **2008**, 5896–5908. (e) Ziener, U. *J. Phys. Chem. B* **2008**, *112*, 14698–14717.

(15) (a) Piguet, C.; Bernardinelli, G.; Hopfgartner, G. *Chem. Rev.* **1997**, *97*, 2005–2062. (b) Albrecht, M. *Chem. Rev.* **2001**, *101*, 3457–3497.

(16) Fujita, M.; Ogura, K. *Bull. Chem. Soc. Jpn.* **1996**, *69*, 1471–1482.

(17) Dawe, L. N.; Shuvaev, K. V.; Thompson, L. K. *Chem. Soc. Rev.* **2009**, *38*, 2334–2359.

(18) (a) Kilpin, K. J.; Paul, U. S. D.; Lee, A. L.; Crowley, J. D. *Chem. Commun.* **2011**, 328–330. (b) Crowley, J. D.; Gavey, E. L. *Dalton Trans.* **2010**, *39*, 4035–4037. (c) Crowley, J. D.; Bandeen, P. H. *Dalton Trans.* **2010**, *39*, 612–623. (d) Chandrasekhar, N.; Chandrasekar, R. *J. Org. Chem.* **2010**, *75*, 4852–4855. (e) Fleischel, O.; Wu, N.; Petitjean, A. *Chem. Commun.* **2010**, *46*, 8454–8456. (f) Zornik, D.; Meudtner, R. M.; El Malah, T.; Thiele, C. M.; Hecht, S. *Chem.—Eur. J.* **2011**, *17*, 1473–1484. (g) Ostermeier, M.; Berlin, M.-A.; Meudtner, R. M.; Demeshko, S.; Meyer, F.; Limberg, C.; Hecht, S. *Chem.—Eur. J.* **2010**, *16*, 10202–10213. (h) Li, Y.; Pink, M.; Karty, J. A.; Flood, A. H. *J. Am. Chem. Soc.* **2008**, *130*, 17293–17295.

(19) Ruiz, J.; Astruct, D. *C. R. Acad. Sci. Paris, Sér. IIc* **1998**, *t1*, 21−27.

(20) Azidoferrocene has been previously prepared from ferrocene by successive lithiation, bromination, and treatment with sodium azide: (a) Dong, T.-Y.; Lai, L.-L. *J. Organomet. Chem.* **1996**, *509*, 131–134. (b) Nesmeyanov, A. N.; Drozd, V. N.; Sazonova, V. A. *Dokl. Akad. Nauk SSSR* **1963**, *150*, 321–324.

(21) Tárraga, A.; Otón, F.; Espinosa, A.; Velasco, M. D.; Molina, P.; Evans, M. D. *Chem. Commun.* **2004**, 458–459.

(22) Sheldrick, G. M. *SADABS: Program for Empirical Absorption Correction of Area Detector Data*; University of Göttingen: Göttingen, Germany, 1996.

(23) Sheldrick, G. M. *SHELX-97: An integrated system for solving and refining crystal structures from diffraction data*; University of Göttingen: Göttingen, Germany, 1996.

(24) Neese, F. *ORCA—an ab initio, density functional and semiempirical program package*, version 2.8.0; Universität Bonn: Bonn, Germany, 2010. Web page: http://www.thch.uni-bonn.de/tc/orca/.

(25) Tight convergence criteria for optimizations in ORCA: energy change 1.0 × 10^{-6} hartree; maximum gradient 1.0 × 10^{-4} hartree/a_0; root-mean-square (rms) gradient 3.0 × 10^{-5} hartree/a_0; maximum displacement 1.0 × 10^{-3} a_0; rms displacement 6.0 × 10^{-4} a_0.

(26) (a) Becke, A. D. *J. Chem. Phys.* **1993**, *98*, 5648–5652. (b) Lee, C. T.; Yang, W. T.; Parr, R. G. *Phys. Rev. B* **1988**, *37*, 785–789.

(27) Neese, F.; Wennmohs, F.; Hansen, A.; Becker, U. *Chem. Phys.* **2009**, *356*, 98–109.

(28) Schaefer, A.; Horn, H.; Ahlrichs, R. *J. Chem. Phys.* **1992**, *97*, 2571–2577.

(29) Weigend, F.; Ahlrichs, R. *Phys. Chem. Chem. Phys.* **2005**, *7*, 3297–3305.

(30) Metz, B.; Stoll, H.; Dolg, M. *J. Chem. Phys.* **2000**, *113*, 2563−2569. ECP parameters for Pb[SD(60,MDF)] have been obtained from the pseudopotential library of the Stuttgart/Cologne group, at http://www.theochem.uni-stuttgart.de/pseudopotentials/.

(31) Schäfer, A.; Huber, C.; Ahlrichs, R. *J. Chem. Phys.* **1994**, *100*, 5829−5835. Basis sets may be obtained from the Basis Set Exchange (BSE) software and the EMSL Basis Set Library: https://bse.pnl.gov/bse/portal. Feller, D. *J. Comput. Chem.* **1996**, *17*, 1571–1586.

(32) (a) Biegler-König, F. W. Schönbohm, J. *AIM2000*, version 2.0, 2002. Home page: http://www.aim2000.de/. (b) Biegler-König, F.; Schönbohm, J.; Bayles, D. C. *Comput. Chem.* **2001**, *22*, 545–559. (c) Biegler-König, F.; Schönbohm, J. *J. Comput. Chem.* **2002**, *23*, 1489–1494.

(33) Frisch, M. J.; Trucks, G. W.; Schlegel, H. B.; Scuseria, G. E.; Robb, M. A.; Cheeseman, J. R.; Scalmani, G.; Barone, V.; Mennucci, B.; Petersson, G. A.; Nakatsuji, H.; Caricato, M.; Li, X.; Hratchian, H. P.; Izmaylov, A. F.; Bloino, J.; Zheng, G.; Sonnenberg, J. L.; Hada, M.; Ehara, M.; Toyota, K.; Fukuda, R.; Hasegawa, J.; Ishida, M.; Nakajima, T.; Honda, Y.; Kitao, O.; Nakai, H.; Vreven, T.; Montgomery, J. A., Jr.; Peralta, J. E.; Ogliaro, F.; Bearpark, M.; Heyd, J. J.; Brothers, E.; Kudin, K. N.; Staroverov, V. N.; Kobayashi, R.; Normand, J.; Raghavachari, K.; Rendell, A.; Burant, J. C.; Iyengar, S. S.; Tomasi, J.; Cossi, M.; Rega, N.; Millam, N. J.; Klene, M.; Knox, J. E.; Cross, J. B.; Bakken, V.; Adamo, C.; Jaramillo, J.; Gomperts, R.; Stratmann, R. E.; Yazyev, O.; Austin, A. J.; Cammi, R.; Pomelli, C.; Ochterski, J. W.; Martin, R. L.; Morokuma, K.; Zakrzewski, V. G.; Voth, G. A.; Salvador, P.; Dannenberg, J. J.; Dapprich, S.; Daniels, A. D.; Farkas, Ö.; Foresman, J. B.; Ortiz, J. V.; Cioslowski, J.; Fox, D. J. *Gaussian 09*, revision A.02; Gaussian, Inc.: Wallingford, CT, 2009.

(34) Wiberg, K. *Tetrahedron* **1968**, *24*, 1083–1096.

(35) Glendening, E. D.; Badenhoop, J. K.; Reed, A. E.; Carpenter, J. E.; Bohmann, J. A.; Morales, C. M.; Weinhold, F. *Using the NBO 5.9 code interfaced to Gaussian09*; Theoretical Chemistry Institute, University of Wisconsin: Madison, WI, 2001.

(36) VMD—Visual Molecular Dynamics; Humphrey, W.; Dalke, A.; Schulten, K. *J. Mol. Graphics*, **1996**, *14*, 33−38. Home page: http://www.ks.uiuc.edu/Research/vmd/.

(37) (a) Fechtenkötter, A.; Sallwächter, K.; Harbison, M. A.; Müllen, K.; Spiess, H. W. *Angew. Chem., Int. Ed.* **1999**, *38*, 3039–3042. (b) Watson, M. D.; Jäckel, F.; Severin, N.; Rabe, J. P.; Müllen, K. *J. Am. Chem. Soc.* **2004**, *126*, 1402–1407. (c) Venkataramana, G.; Sankararaman, S. *Org. Lett.* **2006**, *8*, 2739–2742. (d) Nandy, R.; Subramoni, M.; Varghese, B.; Sankararaman, S. *J. Org. Chem.* **2007**, *72*, 938–944.

(38) (a) Gelin, F.; Thummel, R. P. *J. Org. Chem.* **1992**, *57*, 3780–3783. (b) Saweczko, P.; Kraatz, H.-B. *Coord. Chem. Rev.* **1999**, *190−192*, 185–188. (c) Sadhukhan, N.; Bera, J. K. *Inorg. Chem.* **2009**, *48*, 978–990.

(39) Li^+, K^+, Ca^{2+}, Mg^{2+}, Ni^{2+}, Cd^{2+}, and Pb^{2+} were added as perchlorate salts, while Na^+, Cu^{2+}, Zn^{2+}, and Hg^{2+} were added as triflate salts.

(40) The OSWV technique has been employed to obtain well-resolved potential information, while the individual redox processes are poorly resolved in the CV experiments in which individual $E_{1/2}$ potentials cannot be easily or accurately extracted from these data. (a) Serr, B. R.; Andersen, K. A.; Elliot, C. M.; Anderson, O. P. *Inorg. Chem.* **1988**, *27*, 4499–4504. (b) Richardson, D. E.; Taube, H. *Inorg. Chem.* **1981**, *20*, 1278–1285.

(41) Miller, S. R.; Gustowski, D. A.; Chen, Z: H.; Gokel, G. W.; Echegoyen, L.; Kaifer, A. E. *Anal. Chem.* **1988**, *60*, 2021–2024.

(42) BEF = binding enhancement factor, calculated using the equation $\ln(K_{\mathrm{red}}/K_{\mathrm{ox}}) = \Delta E°(nF/RT)$, where the equilibrium constants K_{ox} and K_{red} correspond to the complexation processes by the oxidized and reduced forms of the ligand. (a) Beer, P. D.; Gale, P. A.; Chen, G. Z. *Adv. Phys. Org. Chem.* **1998**, *31*, 1–90. (b) Beer, P. D.; Gale, P. A.; Chen, G. Z. *Coord. Chem. Rev.* **1999**, *185−186*, 3–36.

(43) Connelly, N. G.; Geiger, W. E. *Chem. Rev.* **1996**, *96*, 877–910.

(44) (a) Caballero, A.; Espinosa, A.; Tárraga, A.; Molina, P. *J. Org. Chem.* **2008**, *73*, 5489–5497. (b) Romero, T.; Caballero, A.; Espinosa, A.; Tárraga, A.; Molina, P. *Dalton Trans.* **2009**, 2121–2129. (c) Zapata, F.; Caballero, A.; Espinosa, A.; Tárraga, A.; Molina, P. *Inorg. Chem.* **2009**, *48*, 11566–11575. (d) Alfonso, M.; Tárraga, A.; Molina, P. *J. Org. Chem.* **2011**, *76*, 939–947.

(45) (a) Marder, S. R.; Perry, J. W.; Tiemann, B. G. *Organometallics* **1991**, *10*, 1896–1901. (b) Coe, B. J.; Jones, C. J.; McCleverty, J. A.; Bloor, D.; Cross, G. J. *J. Organomet. Chem.* **1994**, *464*, 225–232. (c) Müller, T. J.; Netz, A.; Ansorge, M. *Organometallics* **1999**, *18*, 5066–5074.

(46) (a) Sohn, Y. S.; Hendrickson, D. N.; Gray, M. B. *J. Am. Chem. Soc.* **1971**, *93*, 3603–3619. (b) Sanderson, C. T.; Quinian, J. A.; Conover, R. C.; Johnson, M. K.; Murphy, M.; Dluhy, R. A.; Kuntal, C. *Inorg. Chem.* **2005**, *44*, 3283–3289. (c) Gao, L.-B.; Zhang, L.-Y.; Shi, L.-X.; Cheng, Z.-N. *Organometallics* **2005**, *24*, 1678–1684.

(47) (a) Barlow, S.; Bunting, H. E.; Ringham, C.; Green, J. C.; Bublitz, G. U.; Boxer, S. G.; Perry, J. W.; Marder, S. R. *J. Am. Chem. Soc.* **1999**, *121*, 3715–3723. (b) Yamaguchi, Y.; Ding, W.; Sanderson, C. T.; Borden, M. L.; Morgan, M. J.; Kutal, C. *Coord. Chem. Rev.* **2007**, *251*, 515–524.

(48) *Specfit/32 Global Analysis System*; Spectrum Software Associates 1999−2004; http:www.bio−logic.info/spectfitsup/index.html. The Specfit program was acquired from Biologic, SA, in January 2005.

(49) Hirose, K. *J. Inclusion Phenom. Macrocyclic Chem.* **2001**, *39*, 193–209.

(50) Bock, C. W.; Katz, A. K.; Markham, G. D.; Glusker, J. P. *J. Am. Chem. Soc.* **1999**, *121*, 7360–7372.

(51) Marcus, Y. *Chem. Rev.* **1988**, *88*, 1475–1498.

(52) Alberts, I. L.; Nadassy, K.; Wodak, S. J. *Protein Sci.* **1998**, *7*, 1700–1716.

(53) Pavlov, M.; Siegbahn, P. E. M.; Sandström, M. *J. Phys. Chem. A* **1998**, *102*, 219–228.

(54) Szabo, A.; Ostlund, N. S. *Modern Quantum Chemistry. Introduction to advanced electornic structure theory*; Dover Publications: Mineola, NewYork, 1989.

(55) Bader, R. F. W. *Atoms in Molecules: A Quantum Theory*; Oxford University Press: Oxford, U.K., 1990.

(56) The conductivity measurement of a 10^{-3} M solution of $Ni(ClO_4)_2$ in acetonitrile was $\Lambda_M = 425$ (Ω^{-1} cm^2 mol^{-1}), while for the complex, under the same conditions, it was $\Lambda_M = 388$ (Ω^{-1} cm^2 mol^{-1}).

(57) Venkataramani, S.; Jana, U.; Dommaschk, M.; Sönnichsen, Tuczek, F.; Herges, R. *Science* **2011**, *331*, 445–448.

(58) Relevant features for the C_i-symmetric singlet [$\mathbf{6}_2Ni(ClO_4)_2$]: Ni−N3$_t$ bond, $d = 2.076$ Å, WBI = 0.386, LBO = 0.528, $\rho(\mathbf{r}_c) \times 10^2 = 7.14$ e/a_0^3); Ni−N$_p$ bond, $d = 2.115$ Å, WBI = 0.406, LBO = 0.484, $\rho(\mathbf{r}_c) \times 10^2 = 6.71$ e/a_0^3); Ni−O bond, $d = 2.156$ Å, WBI = 0.225, LBO = 0.528, $\rho(\mathbf{r}_c) \times 10^2 = 5.57$ e/a_0^3).

(59) $d_{Ni-N} = 2.099-2.104$ Å; WBI = 0.271−0.272; LBO = 0.506−0.509; $\rho(\mathbf{r}_c) \times 10^2 = 6.66-6.74$ e/a_0^3); $d_{Ni-N} = 2.132-2.137$ Å; WBI = 0.246−0.247; LBO = 0.464−0.464; $\rho(\mathbf{r}_c) \times 10^2 = 6.45-6.46$ e/a_0^3; $d_{Ni-O} = 2.112-2.125$ Å, WBI = 0.271−0.273, LBO = 0.566−0.569, $\rho(\mathbf{r}_c) \times 10^2 = 5.46-5.54$ e/a_0^3; angle N$_p$−Ni−O: 82.6−84.6°; angle N3$_t$−Ni−O: 88.8−89.8.

(60) Relevant features for the C_i-symmetric [$\mathbf{5}\cdot Ni(ClO_4)_2]_2$: Ni−N3$_t$ bonds, $d = 2.071$ and 2.090 Å, WBI = 0.277 and 0.269, LBO = 0.534 and 0.517, $\rho(\mathbf{r}_c) \times 10^2 = 7.29$ and 6.94 e/a_0^3; Ni−N$_p$ bonds, $d = 2.181$ and 2.198 Å, WBI = 0.243 and 0.235, LBO = 0.442 and 0.427, $\rho(\mathbf{r}_c) \times 10^2 = 5.81$ and 5.64 e/a_0^3; Ni−O bonds, $d = 2.090$ and 2.151 Å, WBI = 0.282 and 0.253, LBO = 0.595 and 0.528, $\rho(\mathbf{r}_c) \times 10^2 = 6.03$ and 4.78 e/a_0^3.

(61) (a) Zapata, F.; Caballero, A.; Espinosa, A.; Tárraga, A.; Molina, P. *Org. Lett.* **2008**, *10*, 41–44. (b) Zapata, F.; Caballero, A.; Espinosa, A.; Tárraga, A.; Molina, P. *J. Org. Chem.* **2009**, *74*, 4787–4796.

(62) $d_{Pb-N} = 2.617$, 2.684 Å, WBI = 0.142, 0.136, LBO = 0.435, 0.386, $\rho(\mathbf{r}_c) \times 10^2 = 3.87$, 3.53 e/$a_0^3$; $d_{Pb-O} = 2.531-2.894$ Å, WBI = 0.131−0.071, LBO = 0.468−0.214, $\rho(\mathbf{r}_c) \times 10^2 = 4.02-1.90$ e/a_0^3.

(63) $d_{Pb-N} = 2.914$, 2.959 Å; WBI = 0.096, 0.090; LBO = 0.250, 0.235; $\rho(\mathbf{r}_c) \times 10^2 = 1.93$, 1.80 e/$a_0^3$.